URSI GASS 2020, Rome, Italy, 29 August - 5 September 2020

Electromagnetic Loop Sensor

Christopher G. Hynes* and Rodney G. Vaughan
School of Engineering Science, Simon Fraser University
Burnaby, BC V5A 1S6, Canada. E-mail: c_h@sfu.ca; rodney_vaughan@sfu.ca

Abstract

An electrically small dual-loaded loop is capable of simultaneously detecting orthogonal components of the electric and magnetic fields. When three orthogonal loops are used, the sensor is capable of simultaneously detecting all six electromagnetic components. The response of a dual-loaded loop to an electric field is reformulated and new results are presented. Simulations are used to validate the derived results and excellent agreement is achieved.

1 Background and Introduction

A loop antenna with two antipodal loads is a well known Electromagnetic (EM) field sensor [1]. When the loop is electrically small it can be used to simultaneously detect one component of the electric and magnetic intensity field vectors. By using three orthogonal loops, it is capable of measuring the complete EM vectors (comprising the three electrical and the three magnetic field components). The response of a dual-loaded loop to a linearly polarized plane wave was formulated by Kanda in 1984 [2], who later extended the analysis to the response of centrally located electric and magnetic dipole moments [3]. At the time of the formulations, it was computationally challenging to use simulations, so validation measurements were performed in Large Transverse Electromagnetic (TEM) cells, which lead to significant measurement uncertainties. Some papers that have characterized a dual-loaded loop antenna have reported significant discrepancy between theory and measurements (e.g. [2, 4]), so there is a need to carefully validate the formulations.

This paper reformulates the response to an antipodal dual-loaded loop to an electric field and new results are presented. Specific examples are given for a linearly polarized plane wave and centrally located electric and magnetic dipole moments. Simulations are used to validate the new formulations and excellent agreement is achieved. Such numerical experiments using magnetic and electric dipole moments would be very challenging to perform using a physical set-up. The new formulations correct previously derived results and thereby allow for more accurate measurements of an electromagnetic field when using a dual-loaded loop sensor.

2 Theory

Kanda extended the analysis of a dual-loaded loop sensor for the case of general incident field distributions [2]. In the present work, we rederive Kanda's results using different reasoning and arrive at modified results. Throughout this paper complex notation is used and the time harmonic factor, $e^{j\omega t}$, has been suppressed.

2.1 Single Loop Electric and Magnetic-field Sensor

The boundary conditions on a perfectly conducting loop with two antipodal loads are such that the tangential electric field is zero everywhere except across the loads

$$-I(0)Z_L\delta(\phi) - I(\pi)Z_L\delta(\phi-\pi) = bE^i_\phi(b,\phi) + \frac{j\eta}{4\pi}\int_{-\pi}^{\pi} L(\phi-\phi')I(\phi')d\phi', \quad (1)$$

where b is the loop radius, $\delta(\cdot)$ is the Dirac delta function, η is the wave impedance in the medium and Z_L is the antipodal port impedances. The tangential component of the electric field on the loop surface, E^i_ϕ, the integral kernel, L, and loop current, I, are expressed as Fourier series

$$E^i_\phi(b,\phi) = \sum_{-\infty}^{\infty} f_n e^{-jn\phi} \Rightarrow f_n = \frac{1}{2\pi}\int_{-\pi}^{\pi} E^i_\phi(b,\phi)e^{jn\phi}d\phi, \quad (2)$$

$$I(\phi) = \sum_{-\infty}^{\infty} I_n e^{-jn\phi} \Rightarrow I_n = \frac{1}{2\pi}\int_{-\pi}^{\pi} I(\phi)e^{jn\phi}d\phi, \quad (3)$$

$$L(\phi) = \sum_{-\infty}^{\infty} a_n e^{-jn\phi}, \quad (4)$$

$$a_n = a_{-n} = \frac{kb}{2}(N_{n+1}+N_{n-1}) - \frac{n^2}{kb}N_n, \quad (5)$$

$$N_n = N_{-n} = \frac{1}{\pi}K_0\left(\frac{na}{b}\right)I_0\left(\frac{na}{b}\right) - \frac{1}{2}\int_0^{2kb}(\Omega_{2n}(x) + jJ_{2n}(x))\,dx + \frac{1}{\pi}\left(\ln 4n + \gamma - 2\sum_{m=0}^{n-1}\frac{1}{2m+1}\right), \quad n \neq 0 \quad (6)$$

$$N_0 = \frac{1}{\pi}\ln\frac{8b}{a} - \frac{1}{2}\int_0^{2kb}(\Omega_0(x) + jJ_0(x))\,dx. \tag{7}$$

Ω_n is the Lommel-Weber function, J_n is the Bessel function, $\gamma = 0.5772\cdots$ is Euler's constant, and I_0 and K_0 is the modified Bessel function of the first and second kind, respectively. Substituting (2), (3) and (4) into (1), and performing the integration, yields the Fourier series

$$-I(0)Z_L\delta(\phi) - I(\pi)Z_L\delta(\phi-\pi) = \sum_{-\infty}^{\infty}\left(\frac{j\eta}{2}a_nI_n + bf_n\right)e^{-jn\phi}. \tag{8}$$

The coefficients for this Fourier series are

$$\begin{aligned}\frac{j\eta}{2}a_nI_n + bf_n &= \frac{1}{2\pi}\int_{-\pi}^{\pi}(-I(0)Z_L\delta(\phi) - I(\pi)Z_L\delta(\phi-\pi))\,e^{jn\phi}\,d\phi,\\ &= -\frac{Z_L}{2\pi}(I(0) + I(\pi)e^{n\pi}),\end{aligned} \tag{9}$$

from which the Fourier series coefficients for the loop current are

$$I_n = -\frac{2\pi bf_n}{j\pi\eta a_n} - \frac{Z_L}{j\pi\eta a_n}(I(0) + I(\pi)e^{n\pi}). \tag{10}$$

For electrically small loops, the current can be approximated from the first few Fourier series coefficients (*i.e.* $n < 2$). Using (3) and (10), the difference current between the ports is

$$I_\Delta = I(0) - I(\pi) = 2(I_1 + I_{-1}) = \frac{-2\pi bY_1}{1 + 2Z_LY_1}(f_1 + f_{-1}), \tag{11}$$

where $Y_1 = 2/j\eta\pi a_1$ is the admittance of the $n = 1$ current mode. (11) is different from Kanda [2] in that it doesn't assume that $f_1 = f_{-1}$ and that there is a sign change.

The sum of the port currents is

$$I_\Sigma = I(0) + I(\pi) = 2I_0 = \frac{-4\pi bY_0}{1 + 2Z_LY_0}f_0, \tag{12}$$

where $Y_0 = 1/j\eta\pi a_0$ is the admittance of the $n = 0$ current mode. (12) is different from Kanda [2] by a sign change.

2.1.1 Response to a Linearly Polarized Plane Wave

As shown in Fig.1, the electric intensity for a linearly polarized incident plane wave is denoted

$$\boldsymbol{E}(r) = \boldsymbol{E}_0e^{-j\boldsymbol{k}\cdot\boldsymbol{r}} = E_x\hat{\boldsymbol{x}} + E_y\hat{\boldsymbol{y}} + E_z\hat{\boldsymbol{z}} \tag{13}$$

where,

$$\begin{aligned}\boldsymbol{E}_0 = E_0^i((&-\cos\psi\sin\phi_0 + \sin\psi\cos\theta\cos\phi_0)\hat{\boldsymbol{x}}\\ &+(\cos\psi\cos\phi_0 + \sin\psi\cos\theta\sin\phi_0)\hat{\boldsymbol{y}}\\ &+\sin\psi\sin\theta\hat{\boldsymbol{z}}),\end{aligned} \tag{14}$$

$$\boldsymbol{k} = k(\sin\theta\cos\phi_0\hat{\boldsymbol{x}} + \sin\theta\sin\phi_0\hat{\boldsymbol{y}} - \cos\theta\hat{\boldsymbol{z}}), \tag{15}$$

$$\boldsymbol{r} = x\hat{\boldsymbol{x}} + y\hat{\boldsymbol{y}} + z\hat{\boldsymbol{z}}, \tag{16}$$

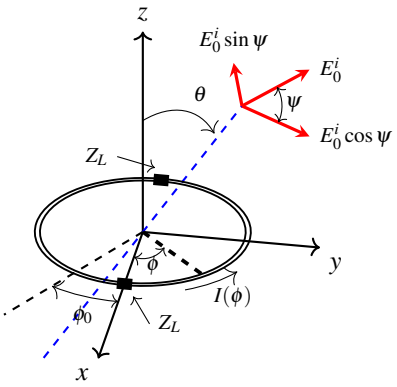

(a) Perspective view.

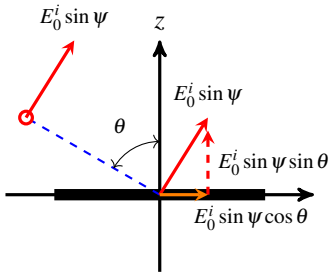

(b) Side view in the plane of incidence.

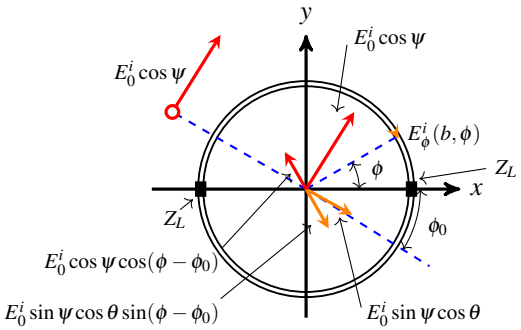

(c) Top view.

Figure 1. Illustration of the linearly polarized plane wave impinging onto a dual-loaded $z-$aligned loop. The loop has a radius of b, conductor radius of a, and antipodal termination impedances of Z_L.

where k is the wavenumber, E_0^i is a complex constant, and $\hat{\boldsymbol{x}}$, $\hat{\boldsymbol{y}}$, and $\hat{\boldsymbol{z}}$ are the Cartesian coordinate unit vectors. As shown in Fig. 1a, ϕ and θ are the spherical coordinates, and ψ is the orientation angle, *i.e.* the angle between the electric intensity and the normal to the plane of incidence.

The magnetic intensity is

$$\boldsymbol{H}(r) = \frac{1}{\eta}\hat{\boldsymbol{k}}\times\boldsymbol{E} = H_x\hat{\boldsymbol{x}} + H_y\hat{\boldsymbol{y}} + H_z\hat{\boldsymbol{z}}, \tag{17}$$

$$\begin{aligned}&= \frac{E_0^ie^{-j\boldsymbol{k}\cdot\boldsymbol{r}}}{\eta}((\cos\psi\cos\theta\cos\phi_0 + \sin\psi\sin\phi_0)\hat{\boldsymbol{x}}\\ &\quad+(\cos\psi\sin\phi_0\cos\theta - \sin\psi\cos\phi_0)\hat{\boldsymbol{y}}\\ &\quad+\cos\psi\sin\theta\hat{\boldsymbol{z}}).\end{aligned} \tag{18}$$

The ϕ component of the electric intensity (14) along a $\hat{\mathbf{z}}-$directed loop of radius b, located at the origin, is

$$E^i_\phi(b,\phi) = E^i_0(\cos\psi\cos(\phi-\phi_0) - \sin\psi\sin(\phi-\phi_0)\cos\theta)\, e^{jkb\cos(\phi-\phi_0)\sin\theta}, \quad (19)$$

$$= \sum_{-\infty}^{\infty} f_n e^{-jn\phi}, \quad (20)$$

where the Fourier coefficient in (20) are given by (2)

$$f_n = -j^{-n}e^{jn\phi_0}\left(\sin\psi\cos\theta\frac{nJ_n(kb\sin\theta)}{kb\sin\theta} + j\cos\psi J_n'(kb\sin\theta)\right). \quad (21)$$

Using the Bessel function relations $J_0'(\cdot) = -J_1(\cdot)$, $J_{-1}(\cdot) = -J_1(\cdot)$ and $J_{-1}'(\cdot) = -J_1'(\cdot)$, and the small argument approximations $J_1(\varepsilon) \approx -\varepsilon/2$ and $J_1'(\varepsilon) \approx 1/2$,

$$f_0 = j\cos\psi J_1(kb\sin\theta) \approx -j\frac{kb}{2}\cos\psi\sin\theta, \quad (22)$$

$$f_1 + f_{-1} = 2\cos\phi_0\cos\psi J_1'(kb\sin\theta) - 2\sin\phi_0\sin\psi\cos\theta\frac{J_1(kb\sin\theta)}{kb\sin\theta}, \quad (23)$$

$$\approx \cos\phi_0\cos\psi + \sin\phi_0\sin\psi\cos\theta. \quad (24)$$

Comparing (22) and (24) to the field expressions for the electric and magnetic intensities (14) and (18), yields

$$I_\Sigma = I(0) + I(\pi) = \frac{j2\pi kb^2\eta Y_0}{1+2Y_0Z_L}H_z, \quad (25)$$

$$I_\Delta = I(0) - I(\pi) = -\frac{2\pi bY_1}{1+2Y_1Z_L}E_y. \quad (26)$$

2.1.2 Response to electric and magnetic dipole moments at the origin

Electric and magnetic dipole moments located at the origin, can be expressed, respectively

$$\boldsymbol{m}_e = I\boldsymbol{\ell} = m_{e,x}\hat{\mathbf{x}} + m_{e,y}\hat{\mathbf{y}} + m_{e,z}\hat{\mathbf{z}}, \quad (27)$$

$$\boldsymbol{m}_m = I\boldsymbol{a} = m_{m,x}\hat{\mathbf{x}} + m_{m,y}\hat{\mathbf{y}} + m_{m,z}\hat{\mathbf{z}}, \quad (28)$$

where m_{ej} and m_{mj} are the components of the electric and magnetic dipole moment along the j^{th} coordinate, respectively, I is the current amplitude, $\boldsymbol{\ell}$ is the electric dipole's incremental length vector, and $\boldsymbol{a}$ is the magnetic dipole's incremental area vector in the direction normal to the loop (following the "right-hand rule" convention). The tangential component of the electric field from these moments on the loop is [3]

$$E^i_\phi = m_{m,z}G_m + m_{e,y}G_e\cos\phi - m_{e,x}G_e\sin\phi, \quad (29)$$

where,

$$G_m = \frac{\eta}{4\pi}\left(\frac{k^2}{b} - \frac{jk}{b^2}\right)e^{-jkb}, \quad (30)$$

$$G_e = -\frac{\eta}{4\pi}\left(\frac{jk}{b} + \frac{1}{b^2} + \frac{1}{jkb^3}\right)e^{-jkb}. \quad (31)$$

The Fourier series coefficients for (29) are

$$f_0 = m_{m,z}G_m, \quad (32)$$

$$f_1 = \frac{m_{e,y}G_e}{2} + \frac{m_{e,x}G_e}{2j}, \quad (33)$$

$$f_{-1} = \frac{m_{e,y}G_e}{2} - \frac{m_{e,x}G_e}{2j}, \quad (34)$$

$$f_1 + f_{-1} = m_{e,y}G_e. \quad (35)$$

Using these coefficients in (12) and (11) relates the sum and difference currents to components of the moments,

$$I_\Sigma = I(0) + I(\pi) = -\frac{4\pi bY_0G_m}{1+2Y_0Z_L}m_{m,z}, \quad (36)$$

$$I_\Delta = I(0) - I(\pi) = -\frac{2\pi bY_1G_e}{1+2Y_1Z_L}m_{e,y}. \quad (37)$$

Note that (37) is half of the value presented in previous work [3, 5], and both (36) and (37) differ from the previous work by a sign change.

3 Results

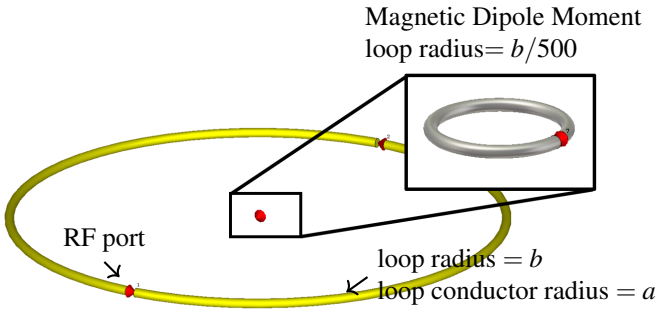

(a) Simulation model with a $\hat{\mathbf{y}}-$directed magnetic dipole source at the centre. In this model the magnetic dipole radius was $b/500$.

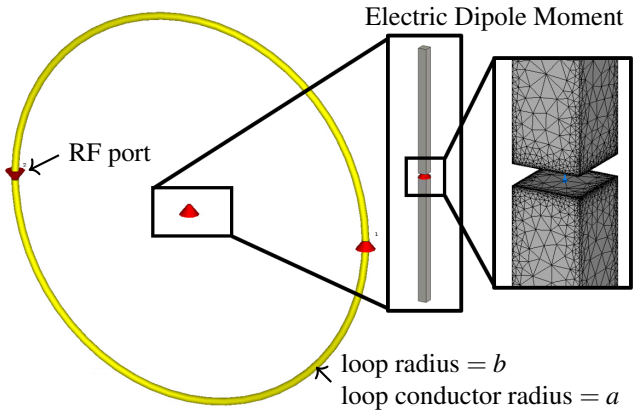

(b) Simulation model with a electric dipole source at the centre. In this model the electric dipole length was $b/83$, the dipole width was $b/7,500$, and the dipole feed gap of $b/25,000$.

Figure 2. Simulation models for a centrally located (a) magnetic and (b) electric dipole moment sources. The loop conductor radius was $a = b/52$, and the port gaps were $2a$.

The formulations were verified by modelling a single dual-loaded loop in CST Microwave Studio, with simulation

models shown in Fig. 2. Three cases were considered: when the loop was excited with 1) a linearly polarized plane wave, 2) a small loop (*i.e.* a magnetic moment), and 3) a small dipole (*i.e.* an electric moment). The results for a plane wave source are shown in Fig. 3a, and good agreement with (25) and (26) is seen when $kb < 0.2$. The results for the magnetic and electric dipole moment sources are shown in Fig. 3b and Fig. 3c, respectively. The results again confirm the derivations presented in this paper, as good agreement is seen when $kb < 1$ and $kb < 0.2$ for a magnetic and electric moment, respectively. Kanda and Hill's formulation for the response of a dual-loaded loop to a centrally located magnetic dipole moment only differs to (36) in a sign change, however an electric source is seen to differ by a factor of 2.

4 Conclusion

The antipodal dual-loaded loop sensor plays a critical part in three-loop antenna systems. The theoretical response of a dual-loaded loop was revisited and new formulations were presented. The modified formulations are validated using simulation with an incident linearly polarized plane wave, and centrally located magnetic and electric dipole moments. The new expressions will result in more meaningful measurements of electromagnetic fields, particularly from electric moment sources, when using a dual-loaded loop sensor.

Acknowledgement

We acknowledge the support of the Natural Sciences and Engineering Research Council of Canada (NSERC), [funding reference number CGSD2-535282-2019].

Cette recherche a été financée par le Conseil de recherches en sciences naturelles et en génie du Canada (CRSNG), [numéro de référence CGSD2-535282-2019].

References

[1] H. Whiteside and R.W.P. King, "The loop antenna as a probe," *IEEE Transactions on Antennas and Propagation*, vol. 12, no. 3, pp. 291–297, May 1964.

[2] M. Kanda, "An electromagnetic near-field sensor for simultaneous electric and magnetic-field measurements," *IEEE Transactions on Electromagnetic Compatibility*, vol. EMC-26, no. 3, pp. 102–110, Aug 1984.

[3] M. Kanda and D. A. Hill, "A three-loop method for determining the radiation characteristics of an electrically small source," *IEEE Transactions on Electromagnetic Compatibility*, vol. 34, no. 1, pp. 1–3, Feb 1992.

[4] L. D. Driver and M. Kanda, "An optically linked electric and magnetic field sensor for poynting vector measurements in the near fields of radiating sources," *IEEE Transactions on Electromagnetic Compatibility*, vol. 30, no. 4, pp. 495–503, Nov 1988.

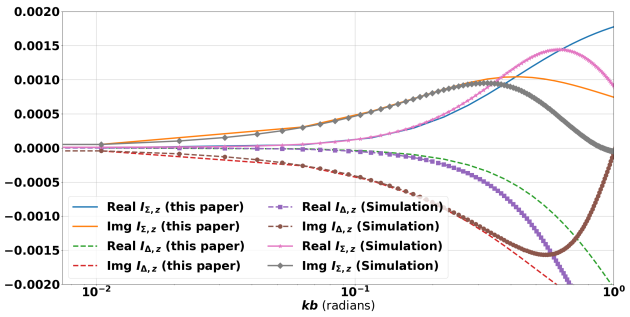

(a) Plane wave source using (25) and (26).

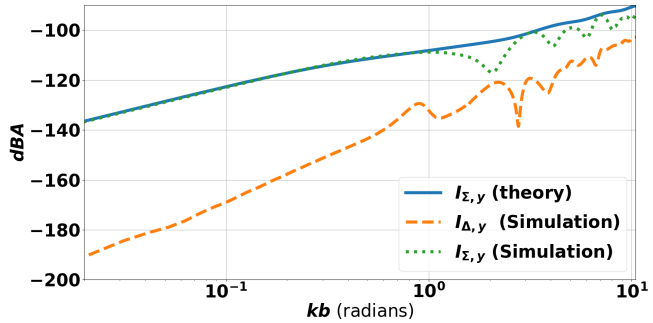

(b) Magnetic dipole moment source. The magnetic dipole radius was $b/500$, fed from a current source of $1A$.

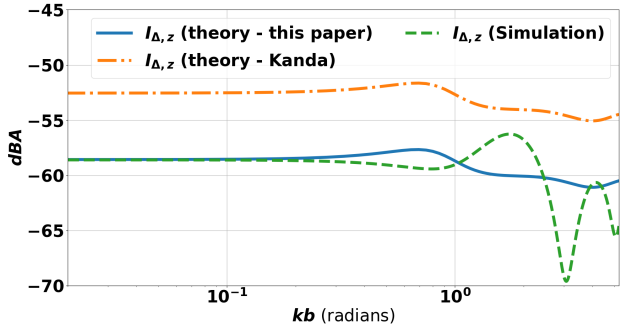

(c) Electric dipole moment source. The electric dipole length was $b/83$, the dipole width was $b/7{,}500$, the dipole feed gap of $b/25{,}000$, and the magnitude was $2.38Amm$ fed from a $1A$ current source.

Figure 3. Simulation results for (a) (25) and (26) with a $1V/m$ plane wave propagating in the $+\hat{\boldsymbol{x}}$ direction with polarization in the $+\hat{\boldsymbol{y}}$ (i.e. $\psi = 0$, $\theta = \pi/2$, and $\phi_0 = 0$), (b) (36) with a magnetic moment source, and (c) (37) with an electric dipole moment source. The port impedances were $Z_L = 315$.

[5] S. Tofani, P. Ossola, G. d'Amore, L. Anglesio, M. Kanda, and D. R. Novotny, "A three-loop antenna system for performing near-field measurements of electric and magnetic fields from video display terminals," *IEEE Transactions on Electromagnetic Compatibility*, vol. 38, no. 3, pp. 341–347, Aug 1996.